ISSN 1063-7761, Journal of Experimental and Theoretical Physics, 2011, Vol. 112, No. 2, pp. 288–302. © Pleiades Publishing, Inc., 2011.
Original Russian Text © S.G. Ovchinnikov, I.A. Makarov, E.I. Shneyder, 2011, published in Zhurnal Eksperimental'noi i Teoreticheskoi Fiziki, 2011, Vol. 139, No. 2, pp. 334–350.

ELECTRONIC PROPERTIES OF SOLID

Effect of Interlayer Tunneling on the Electronic Structure of Bilayer Cuprates and Quantum Phase Transitions in Carrier Concentration and High Magnetic Field

S. G. Ovchinnikov[a,b,*], I. A. Makarov[a], and E. I. Shneyder[a,b]

[a] *Kirensky Institute of Physics, Siberian Branch, Russian Academy of Sciences, Krasnoyarsk, 660036 Russia*

**e-mail: sgo@iph.krasn.ru*

[b] *Reshetnev Siberian State Aerospace University, Krasnoyarsk, 660014 Russia*

Received May 12, 2010

Abstract—We present a theoretical study of the electronic structure of bilayer HTSC cuprates and its evolution under doping and in a high magnetic field. Analysis is based on the t–t'–t''–J^* model in the generalized Hartree–Fock approximation. Possibility of tunneling between CuO_2 layers is taken into account in the form of a nonzero integral of hopping between the orbitals of adjacent planes and is included in the scheme of the cluster form of perturbation theory. The main effect of the coupling between two CuO_2 layers in a unit cell is the bilayer splitting manifested in the presence of antibonding and bonding bands formed by a combination of identical bands of the layers themselves. A change in the doping level induces reconstruction of the band structure and the Fermi surface, which gives rise to a number of quantum phase transitions. A high external magnetic field leads to a fundamentally different form of electronic structure. Quantum phase transitions in the field are observed not only under doping, but also upon a variation of the field magnitude. Because of tunneling between the layers, quantum transitions are also split; as a result, a more complex sequence of the Lifshitz transitions than in single-layer structures is observed.

DOI: 10.1134/S106377611005119X

1. INTRODUCTION

It is well known that all compounds belonging to the class of HTSC cuprates have one or several CuO_2-layers in their structure. It is generally accepted at present that superconductivity and the electronic structure in the vicinity of the Fermi level are determined by the copper–oxygen planes, while the remaining atoms supply charges to these planes. However, the physical properties change with the appearance of two identical CuO_2-layers in $YBa_2Cu_3O_7$ and other cuprates, and primarily the dependence of T_c on the number of the layers points to this fact. The superconducting transition temperature increases with the number n of CuO_2-layers up to $n = 3$, and then decreases [1, 2]. The decrease in T_c for $n > 3$ is traditionally explained by the deficit of carriers per plane. However, the increase in T_c has not yet been adequately explained. In addition, some other effects such as inhomogeneous distribution of doped carriers between the planes [1–10] and the coexistence of the antiferromagnetic and superconducting phases in the same unit cell, but in different planes [11], take place only in multilayer HTSC materials. Therefore, it would be interesting to study the effect of coupling between CuO_2-layers on the properties of cuprates.

The effects associated with the multilayer structure are obviously manifested most dramatically in the superconducting phase. However, it is first necessary to explain how the electronic structure changes upon an increase in the number of layers in the normal phase. Multilayer cuprates, as well as single-layer cuprates, are systems with strong electron correlations; therefore, their description requires a special approach that takes into account the strong repulsion of carriers at the same site. Such an approach is the generalized tight-bonding method of strong coupling proposed in [12–15] and subsequently developed for cuprates [16], manganites [17], and cobaltites [18]. In this approach, the algebra of Hubbard operators is used and analysis is carried out in the language of quasiparticles performing transitions between multielectron initial and final states. Just such approach provides an adequate description of strongly correlated systems. Analogous approaches to describing the normal and superconducting phases based on the Hubbard model, t–J model, and the spin-fermion model in [19–30] in the strong correlation mode give a consistent view of an antiferromagnetic undoped dielectric with a gap associated with charge transfer processes. With doping, the long-range magnetic order is replaced by the short-range order, and the electronic structure for a low doping level is characterized by small hole pockets in the vicinity of points $(\pi/2, \pi/2)$ in the Brillouin zone. The accounting of hole scattering processes from spin fluctuations [21–34] leads to a suppression of the spectral weight of part of the pocket

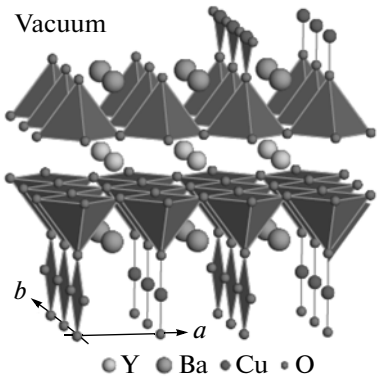

Fig. 1. Unit cell of $YBa_2Cu_3O_7$ bilayer cuprate [32].

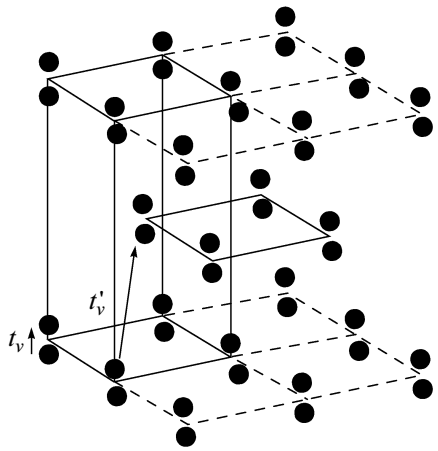

Fig. 2. Schematic of a Bi2212 unit cell: t_v denotes jumps in a bilayer block and t_v' is the jump to the next nearest cell [34].

associated with the shadow zone and to the formation of an arc observed in ARPES [35]. Recent ARPES measurements with an improved energy resolution indeed revealed a pocket with sharply differing spectral weights at different points of the Brillouin zone [36].

Most theoretical publications are made for the CuO_2 plane, and this fact allows to describe single layer cuprates of the type of $La_{2-x}Sr_xCuO_4$ and $Nd_{2-x}Ce_xCuO_4$ directly. However, a considerable part of ARPES experiments and measurements of quantum oscillations was performed on bilayer cuprates. In this connection, it would be interesting to analyze the effect of interlayer tunneling on the electronic structure. The simplest effect of tunneling between the layers has been known for a long time and is associated with the formation of bonding and antibonding bands, which leads to splitting of the Fermi surface manifested most strongly in the vicinity of antinodal points $(\pi, 0)$ [37]. In the present study, the main focus is on the influence of tunneling on the evolution of the Fermi surface upon an increase in doping level and in the magnitude of the high magnetic field. For single-layer cuprates, a series of Lifshitz quantum phase transitions in concentration [38] and in magnetic field [39] is revealed. We will demonstrate the splitting of Lifshitz transitions due to interlayer tunneling.

The structure of the article is as follows. The hopping integral between CuO_2 layers is considered in Section 2. The basic effect of bilayer splitting and its manifestation in the band structure and Fermi surface are also analyzed in this section. We also characterize the concentration evolution of the quasiparticle spectrum and the Fermi surface of bilayer cuprates and demonstrate that it differs insignificantly on a qualitative level from the evolution of single layer structures. In Section 3, the results of our theoretical calculations are compared with the results of ARPES experiments for the Fermi surface and show that the band structures for YBCO and Bi2212 structures with different forms of the hopping integral are very close. In Section 4, the density of states is considered for different concentrations of doped carriers, as well as the concentration dependence of the chemical potential. Section 5 is devoted to the effect of a high external magnetic field on the electronic structure; this problem frequently arises when the results of experiments on quantum oscillations are compared with the ARPES data.

2. BILAYER SPLITTING

The unit cell of $YBa_2Cu_3O_7$ consists of two CuO_5-pyramids formed by a plane CuO_4-cluster and an apical oxygen atom, CuO chains, Y atoms between CuO_2-planes, and Ba atoms (Fig. 1). In our model unit cell, we retain only a bilayer block of two CuO_5-pyramids. Bilayer blocks in adjacent unit cells of the real $YBa_2Cu_3O_7$ compound are arranged precisely one above the other in contrast, for example, to the Bi2212 compound (Fig. 2), in which unit cells are shifted by half their size along the diagonal in the plane. The arrangement of these blocks relative to one another determines the form of the dispersion in the hopping integral along the z axis.

It can be seen from Fig. 1 that the unit cell of a bilayer cuprate is symmetric relative to the reflection in the plane passing through the yttrium atom parallel to the plane of the CuO_2-layer. The wavefunctions for the upper and lower CuO_5-pyramids are identical; therefore, we can consider as an individual pyramid an elementary cluster. This statement would be absolutely valid in the absence of coupling between CuO_2-planes; the presence of jumps between copper oxide layers necessitate the formation of common wavefunctions for the two layers. However, the interlayer jumps are so small that they can be treated as a small perturbation. This allows us to organically inscribe the coupling between CuO_2-layers into the framework of the cluster form of perturbation theory.

The structure of orbital overlapping in the compound under investigation is such that the electron wavefunctions are mainly formed by the states in CuO_2

planes; the probability of a particle transition from one layer to another is very low. The small probability of such transitions is due to the shape of planar $d_{x^2-y^2}$-, p_x-, and p_y-orbitals and a large interplanar spacing. In view of the fact that these orbitals are characterized by a high probability density only in a plane, they play a decisive role in the formation of the electronic structure in an individual CuO_2-layer. Conversely, in the direction perpendicular to the layer, the probability density is very low. The overlap of p_z-oxygen orbitals in which the electron density is mainly concentrated along the z axis is much stronger [40]. The strongest interlayer overlap is observed for s-orbitals of copper and s-orbitals with p-orbitals of oxygen atoms in the neighboring plane. However, the role of s-orbitals is usually ignored because they do not participate in the formation of carrier dynamics in the layer. Nevertheless, the effect of the s–s-overlapping on the electronic structure takes place and is executed directly via plane orbitals of oxygen and, as a consequence, via d-orbitals of copper. This makes possible effective overlapping of d_x-orbitals between CuO_2-planes. This result was demonstrated in [40] using the one-band model. The symmetry of overlapping of the s- and d-orbitals is taken into account in the form of the hopping integral between the layers, which has the following form for $YBa_2Cu_3O_7$:

$$t_\perp = t_{dd}(\cos k_x a - \cos k_y b)^2. \quad (1)$$

In further analysis, during writing the expressions for various points in the **k**-space, we will assume that the equality $a = b = 1$ holds for lattice constants. The value of hopping integral t_{dd} is borrowed from [40] and is assumed to be 0.25 eV (i.e., an order of magnitude smaller than the largest intraplanar hopping integral t_{pd} between d_x-orbitals of copper and p-orbitals of oxygen). After multiplication by the Clebsch–Gordan coefficients and genealogical coefficients appearing upon passage from the description of conventional fermions to Hubbard fermions, the effective jump between the layers becomes 0.1 eV.

The addition of the second apical oxygen atom to a CuO_5-pyramid transforms it into a CuO_6-octahedron, which is chosen as an elementary cluster in the description of the $La_{2-x}Sr_xCuO_4$ one-layer cuprate. The $La_{2-x}Sr_xCuO_4$ one-layer compound was described in detail in [16, 41] using the generalized tight-bonding (GTB) method. In [41] from ab initio calculations, the parameters of the multiband p–d-model were described using the LDA + GTB algorithm (LDA calculations + GTB method [16]) and it was shown that the t–t'–t''–J^*-model is an effective low-energy model. In our calculations, the parameters of the t–t'–t''–J^*-model calculated using the LDA + GTB method are employed in the analysis of the CuO_2 layer [42].

Since HTSC cuprates are systems with strong electron–electron correlations, we reduce the multiband p–d-model with realistic parameters obtained using the LDA + GTB method to the t–J^* model in the low-energy range in the limit $U \gg t$ [43–46]. In this case, U is equal to the energy of the gap with charge transfer $E_{ct} \approx 2$ eV. This model can be written for hole excitations forming quasiparticle bands described by the Hubbard operators

$$X_f^{\sigma S} = |\sigma\rangle\langle S| \text{ and } X_f^{\bar\sigma S} = |\bar\sigma\rangle\langle S|;$$

here, $|\sigma\rangle$ is the local state of a hole with spin projection σ and $|S\rangle$ is the two-hole Zhang–Rice singlet. We will take into account the jumps to other cells up to the third nearest neighbor inclusively; therefore, the t–J^*-model is transformed into the t–t'–t''–J^*-model; J^* indicates that we take into account not only the exchange terms, but also three-center correlated jumps.

It is well known that the generalized tight-bonding method includes the following three stages: exact diagonalization of the intracell part of the Hamiltonian taking into account all interactions in the unit cell, the construction of the Hubbard operators from multiparticle basis states, and allowance for the jumps between cells in perturbation theory. As a result of application of the GTB ideology, the t–t'–t''–J^*-model can be represented in terms of Hubbard operators in the form of intracell and intercell parts. Since a unit cell contains two identical CuO_2 layers with identical wavefunctions, the coupling between these layers belongs to the intercell part of the Hamiltonian and is considered in perturbation theory. Thus, a CuO_5-pyramid is treated as an elementary cluster.

The occupation numbers of single-particle states can be determined by simultaneously solving the equation for the total number of holes,

$$1 + x = \sum_\sigma p_\sigma + 2\langle X^{SS}\rangle,$$

where x is the hole doping level per CuO_2-layer, and the completeness condition of the basis,

$$\sum_\sigma X^{\sigma\sigma} + X^{SS} = 1.$$

The total number of states for the single-particle sector of the Hilbert space is

$$\sum_\sigma p_\sigma = 1 - x.$$

If we take into account the fact that we are considering the paramagnetic phase, the probabilities $p_\sigma = \langle X_f^{\sigma\sigma}\rangle$ and $p_{\bar\sigma} = \langle X_f^{\bar\sigma\bar\sigma}\rangle$ of filling of spin-up and spin-down single-particle states are equal,

$$p_\sigma = p_{\bar\sigma} = \frac{1-x}{2}.$$

The Hamiltonian of the t–t'–t''–J^*-model for a bilayer cuprate has the form

$$H_{t-t'-t''-J^*} = \sum_{f\alpha\sigma}(\varepsilon_1 - \mu)X_{f\alpha}^{\sigma\sigma} + \sum_{f\alpha}(\varepsilon_2 - 2\mu)X_{f\alpha}^{SS}$$
$$+ \sum_{fg\alpha\sigma} t_{fg}X_{f\alpha}^{S\sigma}X_{g\alpha}^{\sigma S} + \sum_{fg\alpha\sigma} J_{fg}(X_{f\alpha}^{\sigma\bar{\sigma}}X_{g\alpha}^{\bar{\sigma}\sigma} - X_{f\alpha}^{\sigma\sigma}X_{g\alpha}^{\bar{\sigma}\bar{\sigma}}) \quad (2)$$
$$- \sum_{m\ln\alpha\sigma} \frac{\tilde{t}_{ml}\tilde{t}_{\ln}}{E_{\rm ct}}(X_{m\alpha}^{S\sigma}X_{l\alpha}^{\sigma\bar{\sigma}}X_{n\alpha}^{\bar{\sigma}S} - X_{m\alpha}^{S\sigma}X_{l\alpha}^{\bar{\sigma}\bar{\sigma}}X_{n\alpha}^{\sigma S}) + H_{\rm bil},$$

in which the term responsible for the coupling between the layers has the form

$$H_{\rm bil} = \sum_{ufd\sigma} t_\perp(X_{fu}^{S\sigma}X_{fd}^{\sigma S} + X_{fd}^{S\sigma}X_{fu}^{\sigma S}).$$

The subscript "α" indicates the upper (u) or lower (d) CuO_2-plane; $J_{fg} = 2\tilde{t}_{fg}^2/E_{\rm ct}$ is the effective exchange interaction parameter associated with jumps to the lower Hubbard band and back; t_{fg} are the intercell intraband jumps between unit cells; $\tilde{t}_k$ are the intercell interband jumps; $E_{\rm ct}$ is the dielectric gap with charge transfer, and ε_1 and ε_2 are the energies of the local states with one and two holes. The values of these parameters (in electronvolts) borrowed from [42] are given below:

$$\varepsilon_2 - \varepsilon_1 = -0.091, \quad E_{\rm ct} = 2,$$
$$t \equiv t_{01} = 0.93, \quad t' \equiv t_{11} = -0.12, \quad t'' \equiv t_{02} = 0.15,$$
$$J \equiv J_{01} = 0.295, \quad J' \equiv J_{11} = 0.003,$$
$$J'' \equiv J_{02} = 0.007, \quad \tilde{t} \equiv \tilde{t}_{01} = 0.77,$$
$$\tilde{t}' \equiv \tilde{t}_{11} = -0.08, \quad \tilde{t}'' \equiv \tilde{t}_{02} = 0.12, \quad t_\perp = 0.1.$$

The above values of parameters of the t–J-model Hamiltonian are typical parameters for the approximation chosen here. In fact, we must speak of a certain interval of possible parameters in the reduction of realistic models (e.g., the multiband p–d-model) to the t–J-model. The variation of parameters in such an interval is mainly associated with the choice of the number of energy levels that will be taken into account in the initial (not yet reduced) Hamiltonian. The calculation of such ranges of parameters was considered in detail in [27, 48].

To determine the quasiparticle excitation spectrum, we use the method of motion equations for the Green function $\langle\langle X_f^\alpha | X_g^{+\beta}\rangle\rangle$ constructed on the Hubbard operators. The reduced Green function is an element of the matrix Green function connected with the electron two-time retarded Green's function $G(\mathbf{r}, E)$ on single-electron operators by the relation

$$G_{\lambda\sigma}(\mathbf{r}, E) = \sum_{\alpha,\beta}\gamma_{\lambda\sigma}(\alpha)\gamma_{\lambda\sigma}^*(\beta)D^{\alpha\beta}(\mathbf{r}, E), \quad (3)$$

in which coefficients $\gamma(\alpha)$ are determined directly by the matrix elements of transition from single-electron operators $a_{f\lambda\sigma}$ to Hubbard operators $X_f^{pq} \equiv X_f^\alpha$:

$$a_{f\lambda\sigma} = \sum_{pq}\langle p|a_{f\lambda\sigma}|q\rangle X_f^{pq}.$$

These matrix elements are calculated in the multielectron basis of states $|p\rangle$ of the unit cell.

The exact equation of motion for operator $X_f^{\sigma S}$ has the form

$$i\dot{X}_f^{\sigma S} = [X_f^{\sigma S}, H] = (\varepsilon_2 - \varepsilon_1)X_f^{\sigma S} + L_f^{\sigma S}; \quad (4)$$

part $L_f^{\sigma S}$ of this equation contains the terms forming the higher-order Green functions. To project these functions onto the basis of single-particle operators, we will use the method of irreducible operators, which is also known as the Mori–Zwanzig projection method employed earlier in [42, 47–49]. In accordance with this method, we separate the one particle contribution proportional to X^β from operator $L_f^{\sigma S}$,

$$L_f^{\sigma S} = \sum_{s\beta} T_f^{(\sigma S)\beta}X_s^\beta + L_f^{\sigma S({\rm irr})},$$
$$T_f^{(\sigma S)\beta} = \langle\{L_f^{\sigma S}, X_s^{+\beta}\}\rangle / \langle\{X_s^\beta, X_s^{+\beta}\}\rangle. \quad (5)$$

Here, $L^{({\rm irr})}$ is the irreducible operator the disregarding of which corresponds to the generalized Hartree–Fock approximation. The overrunning of the mean field approximation was considered in an analogous approach for single-layer cuprates in [29], in which irreducible operators $L^{({\rm irr})}$ lead to dynamic contributions to the mass operator $\Sigma(\mathbf{k}, \omega)$ describing scattering of Hubbard fermions on the spin fluctuations. It is the imaginary part Σ that ensures the suppression of the spectral weight in a part of the hole pocket. In our analysis, we disregard the irreducible contribution and confine ourselves to the generalized Hartree–Fock approximation, in which we can take into account static spatial correlations and describe the dependence of the band structure on the concentration and high magnetic field. However, as shown in [25, 50], allowance for the spectral weight redistribution using the extended set of basis operators leads, strictly speaking, not only to a change in the spectral function for holes, but also to a change in the concentration dependence of the electronic structure of the Fermi surface. For this reason, the values of critical concentrations obtained here may be slightly changed in a more rigorous theory and are rather of qualitative nature.

The kinetic and spin correlators $\langle X_f^{S\sigma}X_g^{\sigma S}\rangle$ and $\langle X_f^{\sigma\bar{\sigma}}X_g^{\bar{\sigma}\sigma}\rangle$ separated in the process of averaging are important characteristics of the system, which determine to a considerably extent the electronic structure [42, 47, 49]. We will use the spin correlation functions

that were calculated self-consistently in [42, 49] for a single-layer cuprate also using the method of irreducible operators. The spin correlators define the short-range antiferromagnetic order in this compound. The kinetic correlators can be calculated self-consistently with a chemical potential with the help of the spectral representation of the Green's function,

$$\langle\langle X_{\mathbf{k}}^{\sigma S} | X_{\mathbf{k}}^{S\sigma} \rangle\rangle = \frac{p_\sigma + x}{2}\left(\frac{1}{E - E_+(\mathbf{k})} + \frac{1}{E - E_-(\mathbf{k})}\right), \quad (6)$$

whose poles $E_+(\mathbf{k})$ and $E_-(\mathbf{k})$ determine the dispersion dependences of antibonding and bonding bands formed as a result of splitting of the quasiparticle band (for example, with spin $\bar{\sigma}$) belonging to the single CuO_2-plane due to interlayer tunneling. The values of the poles are defined as

$$E_\pm(\mathbf{k}) = \varepsilon_2 - \varepsilon_1 - \mu + (p_\sigma + x)t_{\mathbf{k}} + p_{\bar{\sigma}}J_0 + p_{\bar{\sigma}}(p_\sigma + x)\frac{\tilde{t}_{\mathbf{k}}^2}{E_{\mathrm{cl}}} + \Sigma(\mathbf{k}) \pm \varepsilon_\perp, \quad (7)$$

where $\Sigma(\mathbf{k})$ is the mass operator, and the expression

$$\varepsilon_\perp(\mathbf{k}) = (p_\sigma + x)t_\perp(\mathbf{k}) + \frac{3}{2}\frac{t_\perp(\mathbf{k})C_\perp(\mathbf{k})}{p_\sigma + x} \quad (8)$$

characterizes the energy of band splitting due to interlayer tunneling. A band splitting equal to $2\varepsilon_\perp$, which is known as the bilayer splitting, was confirmed in many experiments [35, 41–56]; this property is apparently the main bilayer effect in the normal phase. The mass operator is defined as

$$\Sigma(\mathbf{k}) = \frac{1}{p_\sigma + x}\frac{1}{N}\sum_{\mathbf{q}}[Y_1(\mathbf{k}, \mathbf{q})K_{\mathbf{q}} + Y_2(\mathbf{k}, \mathbf{q})C_{\mathbf{q}} + t_\perp(\mathbf{q})K_{\perp\mathbf{q}}], \quad (9)$$

where N is the number of vectors in the reciprocal space, and coefficients $Y_1(\mathbf{k}, \mathbf{q})$ and $Y_2(\mathbf{k}, \mathbf{q})$ are defined by the expressions

$$Y_1(\mathbf{k}, \mathbf{q}) = t_{\mathbf{q}} - p_\sigma J_{\mathbf{k}-\mathbf{q}} - x\frac{\tilde{t}_{\mathbf{q}}^2}{E_{\mathrm{ct}}} - (p_\sigma + x)\frac{2\tilde{t}_{\mathbf{q}}\tilde{t}_{\mathbf{k}}}{E_{\mathrm{ct}}},$$

$$Y_2(\mathbf{k}, \mathbf{q}) = t_{\mathbf{k}-\mathbf{q}} - p_\sigma J_{\mathbf{q}} + p_\sigma\frac{\tilde{t}_{\mathbf{k}-\mathbf{q}}^2}{E_{\mathrm{ct}}} - (p_\sigma + x)\frac{2\tilde{t}_{\mathbf{k}}\tilde{t}_{\mathbf{k}-\mathbf{q}}}{E_{\mathrm{ct}}}.$$

In the expressions for the band energy, $K_\perp$ and $C_\perp$ are interlayer kinetic and spin correlators. These terms, which are responsible for the additional coupling between the planes, are manifested during decoupling of the equations of motion for bilayer cuprates. The interlayer kinetic correlators can be calculated self-consistently together with the remaining intraplanar kinetic correlators and the chemical potential. As regards the spin correlators, they can be estimated from the following simple consideration: the spin correlators are proportional to the effective exchange integral, $J_\perp \sim 2t_\perp^2/E_{\mathrm{ct}}$. The sign of the spin correlator, which determines the types of correlations between the spins of adjacent layers, was found by exact diagonalization of a bilayer cluster. We considered a unit cell of a bilayer cuprate, consisting of two CuO_5-pyramids, in which all interactions were taken into account exactly. Then the state with the lowest energy was singled out in the resultant basis of two-particle states. Since it turned out to be a singlet state, the ground state in the case when each layer contains only one hole corresponds to the antiferromagnetic state of the two layers. The antiferromagnetic ordering of spins was confirmed experimentally in [57] with the help of neutron diffraction. Doping rapidly destroys the antiferromagnetic order along the c axis, but this does not apply to the antiferromagnetically correlated pair of CuO_2-layers forming the unit cell of bilayer cuprates. Correlations between unit cells are broken. The spin correlation function for the nearest neighbors in a CuO_2-layer is $C_{01} \approx -0.2$ [42], while our calculations of $C_\perp$ based on exact diagonalization of the $(CuO_5)_2$-bipyramid give $C_\perp \approx -0.1$.

Pay attention to the fact of using the assumption that doped carriers are distributed uniformly between the planes so that we have the same number x of carriers in the two planes. In most experimental works, precisely the value of x per CuO_2 is determined.

It follows from formula (1) and Fig. 3 that bilayer splitting depends to a considerable extent on the wavevector. This splitting is zero in the nodal direction and attains its maximal value in the antinodal direction.

Doping affects the electronic structure of cuprates in a more complex view as compared to, for example, metals, for which the hard band model is operative. In the compounds under investigation, the addition of carriers not only increases the number of filled states in the **k**-space, but also changes the dispersion relation itself. This is due to the fact that the quasiparticle energy depends on the filling factor $F = (1 + x)/2$ (i.e., on the number of states for the given band), which in turn is a function of doping level x. For this reason, the band structure exhibits evolution upon doping. In the range of weakly doped compounds, the Fermi surface consists of four elements each of which is formed by two hole pockets embedded into each other (see Fig. 3a). The first quantum phase transition occurs for $x_{c1} = 0.14$ (Fig. 3b). At this point, wider pockets merge into one, which gives rise to an outer hole pocket and the inner electron pocket embedded in it. Along with the newly formed pockets, four growing pockets also exists; they merge for $x_{c2} = 0.18$. As a result, we are left with two hole and two electron pockets, each of which exhibit interlayer splitting at antinodal points (Fig. 3d). Upon a further increase in the doping level, the inner electron pockets collapse and become less and less distinguishable from each other (Fig. 3e). In the vicinity of $x_{c3} = 0.26$, the electron pockets disappear upon a subsequent quantum phase transition, and only two large hole

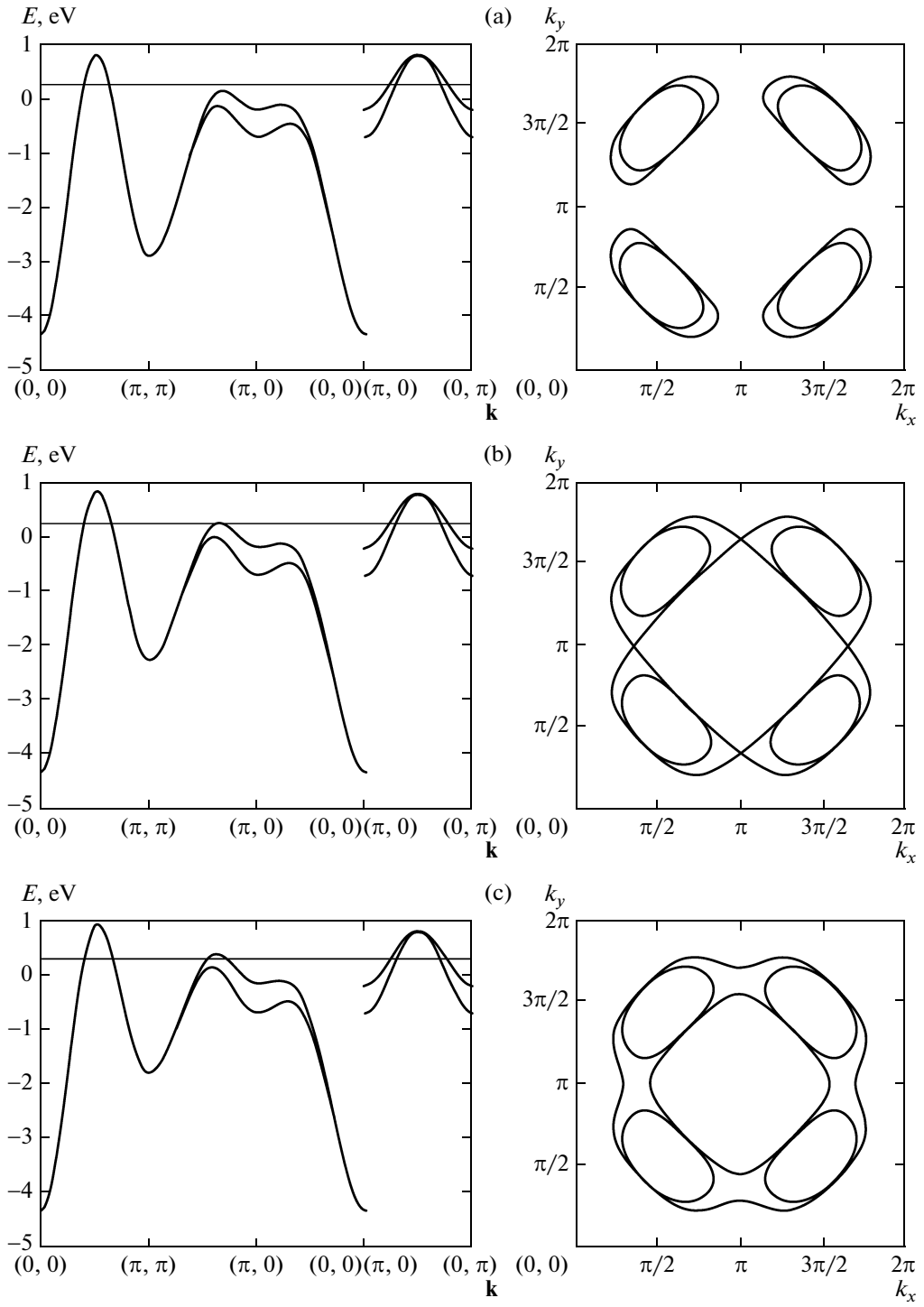

Fig. 3. Evolution of the electronic structure of bilayer cuprates upon doping: (a) $x = 0.11$; (b) $x = 0.14$; (c) $x = 0.16$; (d) $x = 0.18$; (e) $x = 0.22$; and (f) $x = 0.28$. The horizontal line on the diagrams shows the chemical potential level.

pockets are left (Fig. 3f). Naturally, there should be two critical points, but the electron pockets are split so weakly that these critical points cannot be distinguished. Upon an increase in x, antiferromagnetic correlations become weaker, and this is manifested in an increase in energy at point (π, π), indicating the return to the paramagnetic state. It should be noted that the picture of topological variations of the Fermi surface of a double-layer cuprate is almost the same as for a single-layer cuprate. The main difference is associated with the splitting of the Lifshitz transition near the optimal doping level into two transitions at x_{c1} and x_{c2}.

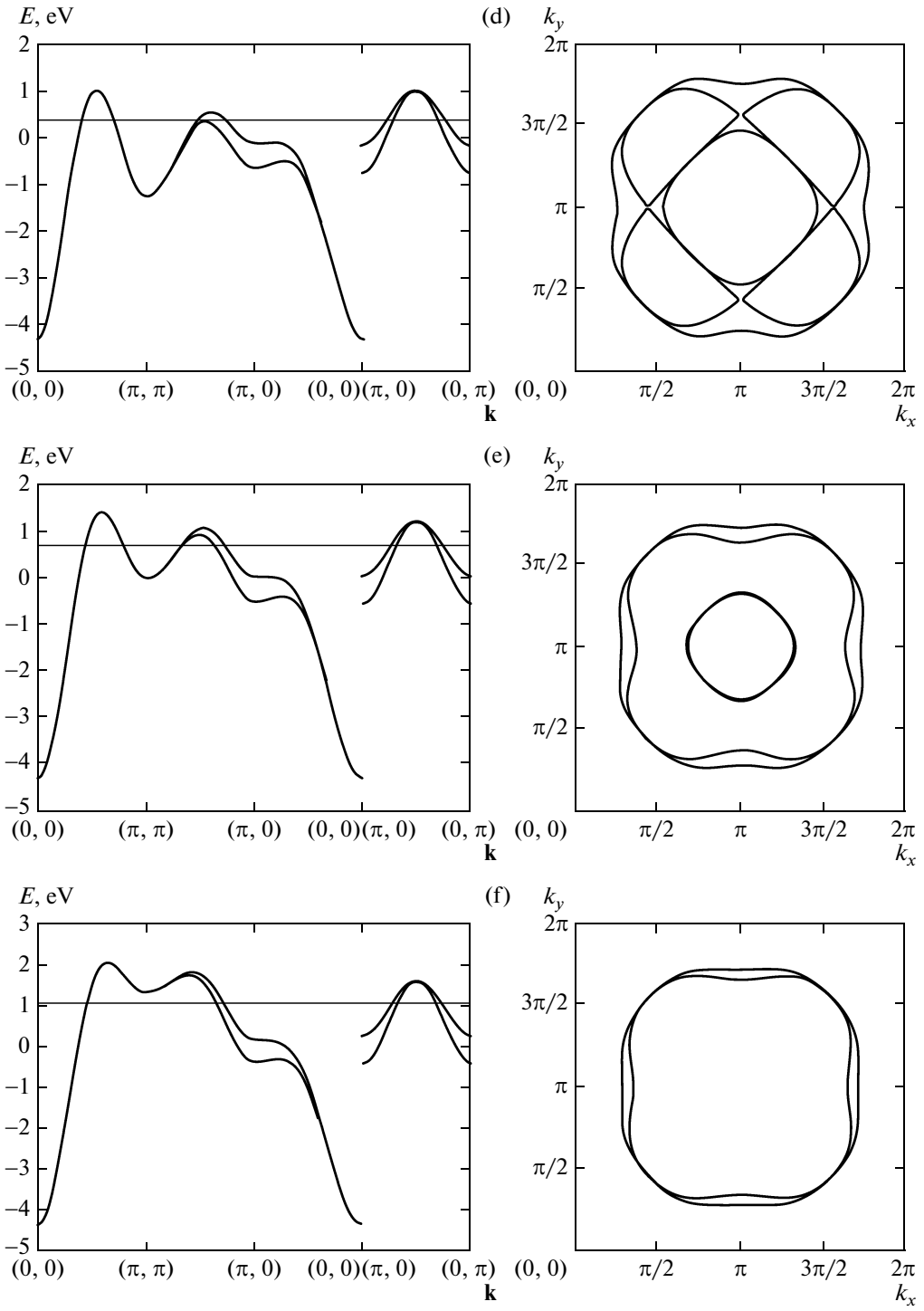

Fig. 3. (Contd.)

The appreciable width (4.5 eV) of the quasiparticle band is due to the use of the t–J-model, which is an effective low-energy model for cuprates. In more realistic models such as the spin–fermion [25] and multiband p–d-model [16], the width of the quasiparticle band, which is clearly observed in ARPES experiments, is typically 0.7 eV. The difference between these models is that the band intersected by the Fermi level in realistic models corresponds to a certain species of quasiparticles with their initial and final states, while in the t–J-model, an additional energy supplementing and broadening the single band appears due to allowance for the presence of the second band in the form of effective jumps to this band and back. The top

of the band obtained in the realistic models is the same as the top of the wide band in the t–J-model, and since we are mainly interested in the states near the Fermi level, while the state in the bulk of the band are less important for our analysis, the approach used here is more or less justified.

3. COMPARISON OF THE RESULTS OF THEORETICAL CALCULATIONS WITH EXPERIMENTAL DATA

The correctness of our calculations is verified by comparing the calculated Fermi surfaces with the results of ARPES experiments. The ARPES method is undoubtedly a powerful tool for studying the electronic structure of materials; however, like any other method, it requires a correct interpretation. For the $YBa_2Cu_3O_7$ bilayer cuprate in the range of weakly doped compositions ($x = 0.11$), ARPES predicts a Fermi surface in the form of arcs (Fig. 4a). The relation between pockets and arcs was discussed in the Introduction; therefore, we compare the pockets calculated by us with the ARPES arc, which are part of a pocket with a high spectral intensity. It can be clearly seen that the highest intensity of the arc coincides with the inner part of the hole pocket obtained in our calculations. For strongly doped compounds, the area of the hole pocket obtained in theoretical calculations is slightly smaller than the area of an analogous part of the ARPES Fermi surface (Fig. 4b); however, their shapes are quite similar. The discrepancy in the areas can be due to the fact that the concentration $x = 0.28$ of doped carriers corresponds to the region in which the strong electron correlation limit is inapplicable.

Since recently, quantum oscillations have been observed in HTSC cuprates [58]. In recent publications devoted to the $YBa_2Cu_3O_7$ compound [59], the existence of four different oscillations instead of one-type oscillations in earlier experiments has been reported. The authors of [59] interpret this result as a consequence of the existence of several segments (or several bands) on the Fermi surface, two of which are associated with bilayer splitting, and the other two, with jumps between unit cells along the z axis. Each Fermi surface corresponds to its own oscillation frequency proportional to the Fermi surface area. Knowing the ratio of the oscillation frequencies associated with splitting, we also know the ratio of the areas of the 2D Fermi surfaces formed by the bonding and antibonding bands. By varying the parameter of the hopping integral between the CuO_2-layers, we can attain the required ratio of the areas. The hopping parameter determined in this way is precisely the required coupling between the layers in the bilayer cuprate. Having performed the above operations with the results of our calculations and using the frequency ratio from [59], we find that the hopping integral required for the fulfillment of the ratio must be $t_\perp = 80$ meV, which is close to the value $t_\perp = 100$ meV used in our analysis.

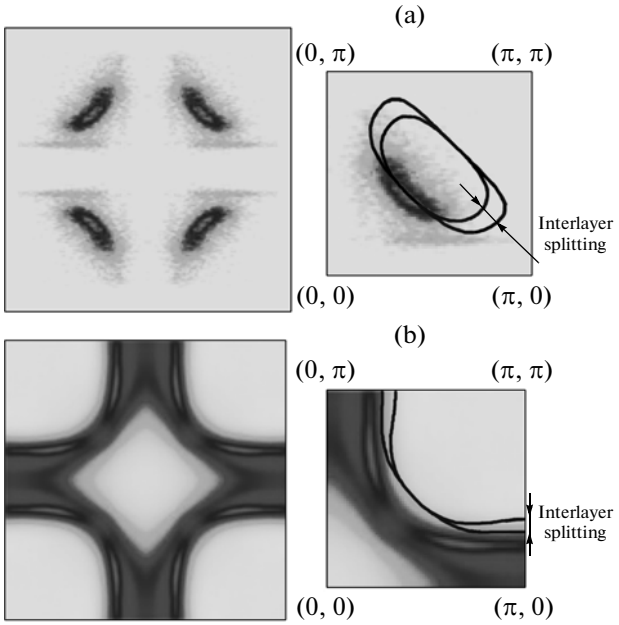

Fig. 4. Comparison of ARPES data [35] for the Fermi surface and the results of theoretical calculations (dark curves) for $YBa_2Cu_3O_7$ bilayer cuprate: (a) $x = 0.11$; (b) $x = 0.28$.

The value of parameter $t_\perp$ calculated in [59] was 8 meV. Such a difference between the values of the hopping integral obtained by us and the authors of the experimental work is not surprising if we take into account that the results of experiments in [59] were interpreted using the theory of free electrons. In the band theory, the spectral density of each point on the dispersion surface (we consider the case without damping) is defined by a delta function with a coefficient of unity. The particles in the band theory do not interact with one another, which is reflected in the equal probabilities of an empty state being filled by a particle and of the addition of a particle to the state that has already been occupied by another particle. Systems with strong electron correlations are described in the language of quasiparticles which have different spectral weights depending on the specific initial and final states, the transition between which is characterized by a quasiparticle. The physical features of such strongly correlated systems are described in terms of the Hubbard operator algebra (in particular, using the Hubbard model). With the help of Hubbard operators, it is possible to single out the filling factors depending on the occupation numbers of the initial and final states. The filling factor, which is always smaller than unity for a certain quasiparticle band, serves as the coefficient in the expression for the spectral density of quasiparticles. Thus, to accumulate the required total number of quasiparticles, a much larger number of states in the k-space are required as compared to quasiparticles behaving in accordance with the laws for a Fermi liquid. This explains the larger area of the Fermi

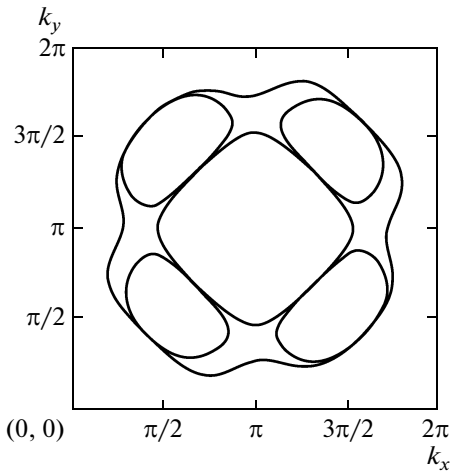

Fig. 5. Fermi surface for Bi2212 bilayer compound with dispersion $k_z = 0$ and doped hole concentration $x = 0.16$.

surface. The better agreement between the hopping integral required for satisfying the ratio of oscillation frequencies and the value used in our analysis as compared to the hopping integral in the band approach indicates that weakly doped HTSC cuprates are described more correctly as systems with strong electron correlations.

The electronic structure obtained for $YBa_2Cu_3O_7$ is generally typical of most bilayer compounds. We consider, for example, the $Bi_2Sr_2CaCu_2O_8$ (Bi2212) compound, for which the hopping integral was obtained in [37]. In this compound, bilayer blocks in neighboring unit cells are shifted along the z axis by half the unit cell diagonal in the ab plane; therefore, we can expect a certain dispersion along the z axis. The authors of [37] obtained the following expression for the hopping integral using the fitting to LDA ab initio calculations:

$$\begin{aligned} E_z &= T_z(k_\parallel, k_z)[(\cos k_x a - \cos k_y b)^2], \\ T_z &= \sqrt{t_{dd}^2 + A_z^2 + 2t_{dd}A_z\cos\frac{k_z c}{2}}, \\ A_z &= 4t_z\cos\left(\frac{k_x a}{2}\right)\cos\left(\frac{k_y b}{2}\right). \end{aligned} \tag{10}$$

The absolute value of k_z-dispersion is determined by parameter t_z; however, since this parameter characterizes the jump between unit cells along the z axis, it is obviously very small and dispersion is weakly distinguishable. Typical values of the parameters for Bi2212 are as follows: $t_{dd} = 0.1$ eV and $t_z = 0.03$ eV [37].

When dispersion along the k_z axis is taken into account in the expression for the hopping integral, the band structure does not change radically; only an insignificant fluctuation of the peak in the $(\pi, 0)$–$(0, 0)$ direction can be noticed upon the variation of k_z from 0 to 2π. The amplitude of this fluctuation depends on the intercell hopping integral in the direction of the z axis; since the value of t_z is much smaller than even t_{dd}, we can hardly expect a noticeable change in the quasiparticle energy. When the dispersion in k_z is activated, the 3D Fermi surface becomes "twisted." The Fermi contour is elongated along the $(\pi, 0)$–$(0, \pi)$ direction for $k_z = 0$ (Fig. 5) and along the $(0, 0)$–(π, π) direction for $k_z = 2\pi$ (Fig. 5c). No other changes are observed on the 2D Fermi surface because the chemical potential does not attain the above-mentioned fluctuating peak in the entire range of doped carrier concentration, for which the generalized tight-bonding method is applicable.

4. DENSITY OF STATES

The critical doping points x_{c1}, x_{c2}, and x_{c3} are characterized by a sharp variation in the topology of the Fermi surface corresponding to the given doping level. In the rigid band model, all features that are determined by the chemical potential for any number of charge carriers can be predicted from the image of the dispersion surface for a certain doping level, while doping in strongly correlated systems changes the dispersion relation also. For this reason, a change in the doping level also shifts the chemical potential as well as the band itself. This fact must be reflected in the form of the dependence of the positions of singularities in the density of states on doping. The formation of new elements of the surface or, in other words, filling of the cavities initiates a jump in the density of states. Since the bands are filled with holes, the density of states also corresponds to holes. The expression for the density of states has the form

$$\begin{aligned} N(E) &= \frac{1}{N}\sum_{\mathbf{k}} A(\mathbf{k}, E) \\ &= -\frac{1}{\pi}\sum_{\mathbf{k}mn}\gamma_\lambda(m)\gamma_\lambda^*(n)\mathrm{Im}D^{m,n}(\mathbf{k}, E + i\delta). \end{aligned} \tag{11}$$

Figure 6 shows the densities of states for different hole concentrations. Filling of the hole states begins from the top of the valence band for electrons. It can be seen that with decreasing energy, the density of states changes jumpwise from zero to a certain value, after which it increases with the hole energy. As well, it should be noted that hole pockets are filled at this stage. For low concentrations $x = 0.05$ and 0.1 in Fig. 6, as well as for $x = 0.11$ in Fig. 3a, the interlayer splitting is located in the filled part of the band deep beneath the Fermi level. At point $x_{c1} = 0.14$, carriers at the boundary of the Brillouin zone fill the neck between the pockets, which appears as the formation of a bridge between the neighboring regions on the Fermi surface. First, a bridge is formed at the antibonding band from the two bands split as a result of tunneling. This antibonding band is a sheet of the open Fermi surface. Soon (at $x_{c2} = 0.18$), the bridge is formed for the bonding band. Both sharp increments

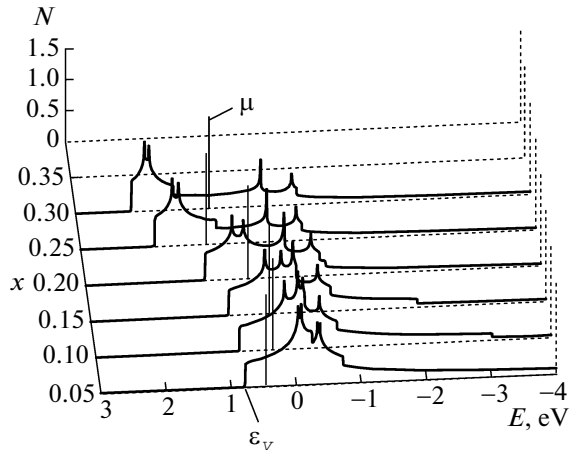

Fig. 6. Density of states of a bilayer cuprate. Vertical lines show the position of the Fermi level; the top of the valence band is shown by an arrow with ε_V.

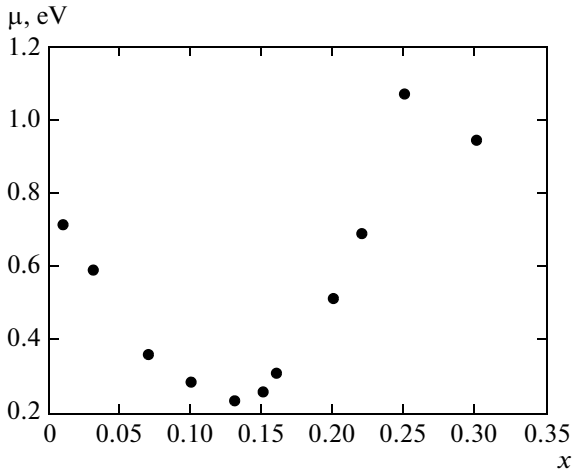

Fig. 7. Dependence of the chemical potential of electrons on the hole doping level.

of the hole density correspond to two van Hove singularities in Fig. 6. The change in the coherency of the Fermi surface leads to a logarithmic singularity in the density of states. It could be expected that a further increase in the doping level would give rise to two jumps and two logarithmic peaks owing to the band structure. However, a rapid increase in the energy is observed instead at point (π, π). This is due to an increase in the number of carriers and, as a result, an increase in the kinetic energy, which suppresses spin correlations and reduces their contribution to the energy of the band. Thus, the short-range antiferromagnetic order gradually disappears. As a consequence, for the number of carriers sufficient for strong correlations, the Fermi level does not fall at the peaks formed due to the states in the vicinity of antinodal point $(\pi, 0)$. In the strongly doped region (see Figs. 3e, 3f), interlayer tunneling is manifested weakly in the form of the Fermi surface. As in single-layer cuprates [42], the Fermi layer reaches the saddle point in the vicinity of $(\pi, 0)$ and the Fermi surface changes its sign (from hole to electron polarity) at too high doping levels $x \approx 0.5$. In this range, the description of cuprates by the t–J-model is disputable.

It follows from the view of the density of states that the chemical potential changes nonlinearly upon an increase in the concentration of doped carriers. Figure 7 shows this dependence in greater detail. The chemical potential first decreases and attains its minimal value near $x = 0.15$, and then increases with the doping level. This increase continues to a level of $x = 0.26$, after which a decrease in the chemical potential is observed again. Such a dependence indicates that some concentration ranges are more advantageous from the energy point of view and, hence, the probability of their realization in the substance is higher. This implies the possibility of phase separation in the crystal, which is often observed in actual practice. For example, the stripes are known to be present in HTSC cuprates.

The density of states obtained in our analysis for $x = 0.25$ can be compared with the results obtained in [60], in which the hole spectrum of two CuO_2-planes was investigated using the two-band model for a magnetic polaron. Bilayer splitting of the density of states observed in [60] for $x = 0.24$ due to the presence of bonding and antibonding bands is qualitatively identical to that calculated in our analysis.

5. QUANTUM PHASE TRANSITIONS IN A HIGH MAGNETIC FIELD

Attempts to conform the shapes of the Fermi surfaces for cuprates predicted by different ARPES experiments have underway for a long time. For strongly doped compounds, most researchers obtained a large Fermi surface around (π, π) of presumably hole type, but in the range of weakly doped compounds, their opinions differ. The disagreement is mainly between the advocates of arcs with an intensity peak in the nodal direction and those supporting small pockets. After publications devoted to quantum oscillations, it has become possible to compare the ARPES data with the area of the Fermi surface calculated using the frequency of quantum oscillations [58]. The discrepancy between the actual doping level and that derived from the calculated area of the Fermi surface indicates that regions of the electron type can exist on it. The same conclusion was drawn in [61], in which it was shown that the Hall constant changes its sign upon cooling; this implies the change in the type of the majority carried. However, it is impossible to directly compare the ARPES data with the results obtained using quantum oscillations and the Hall effect because the latter appear in an external magnetic field. The presence of filling numbers and spin correlators in the

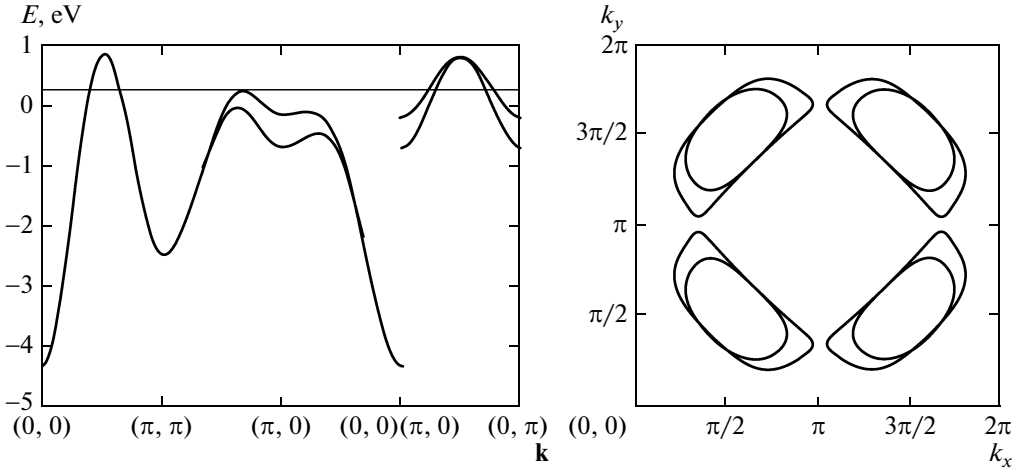

Fig. 8. Band structure (for holes) for the paramagnetic phase ($x = 0.13$).

dispersion relations for strongly correlated electrons leads to a new strong mechanism of variation of the electronic structure upon the application of an external magnetic field. Therefore, it is not obvious beforehand that the Fermi surface in a strong field (quantum oscillations) coincides with the Fermi surface in zero field (ARPES). Consequently, it is necessary to investigate the effect of an external field on the electronic structure. In line with [39], in which this effect was studied for single-layer cuprates, we will analyze the case when the magnetic field is applied to a double-layer cuprate.

We will operate with the approximation of an external field strong enough to order all spins at lattice sites in the same direction, while the spin flip to the state with the opposite spin projection is possible due to a finite temperature. The spin orientation in adjacent planes is naturally not antiferromagnetic any longer, but is ferromagnetic. Under the action of the field, the single-particle state, which is doubly degenerate in energy in the paramagnetic phase, splits into states $|\sigma\rangle$ and $|\bar{\sigma}\rangle$ with energies $\varepsilon_1 - \mu_B H$ and $\varepsilon_1 + \mu_B H$. Correction $\mu_B H$ is associated with the interaction of the spin with the magnetic field and is insignificant (on the order of 0.01 eV) even in a field of 300 T. Therefore, the presence of the magnetic field will be mainly manifested in the characteristic filling of single-particle states and in the form of the spin correlation functions.

If we assume that the spin with projection σ is directed along the field, the occupation number for a state with such a projection is $p_\sigma = \langle X_f^{\sigma\sigma}\rangle = (1 - n_0)(1 - x)$, while the occupation number for the spin-down state is $p_{\bar{\sigma}} = \langle X_f^{\bar{\sigma}\bar{\sigma}}\rangle = n_0(1 - x)$, where n_0 is the concentration of spins antiparallel to the field at a certain temperature:

$$n_0 = \frac{1}{1 + \exp(2\mu_B H/kT)}. \tag{12}$$

Since we assume that the field applied to the compound under investigation is strong enough to orient all spins in the same direction, we assume that the spin correlators are of the ferromagnetic type and are independent of distance:

$$\langle X_f^{\sigma\bar{\sigma}} X_g^{\bar{\sigma}\sigma}\rangle = 0,$$
$$\langle X_f^{\sigma\sigma} X_g^{\sigma\sigma}\rangle = p_\sigma^2.$$

The kinetic correlators can be calculated self-consistently with the help of the spectral theorem for the Green function's:

$$\langle\langle X_{\mathbf{k}}^{\sigma S} | X_{\mathbf{k}}^{S\sigma}\rangle\rangle = \frac{p_\sigma + x}{2} \times \left(\frac{1}{E - E_{\bar{\sigma}+}(\mathbf{k})} + \frac{1}{E - E_{\bar{\sigma}-}(\mathbf{k})}\right), \tag{13}$$

where the expression

$$E_{\bar{\sigma}+}(\mathbf{k}) = \varepsilon_2 - \varepsilon_1 - \mu_B H - \mu + (p_\sigma + x)t_{\mathbf{k}} + p_{\bar{\sigma}}J_0 + p_{\bar{\sigma}}(p_\sigma + x)\frac{\tilde{t}_{\mathbf{k}}^{0S2}}{E_{st}} + \Sigma_{\mathbf{k}} + \varepsilon_\perp \tag{14}$$

characterizes the dispersion of quasiparticles with spin $\bar{\sigma}$ (transition from the single-particle state with spin σ to the singlet state) for the antibonding band, while the expression

$$E_{\bar{\sigma}-}(\mathbf{k}) = \varepsilon_2 - \varepsilon_1 - \mu_B H - \mu + (p_\sigma + x)t_{\mathbf{k}} + p_{\bar{\sigma}}J_0 + p_{\bar{\sigma}}(p_\sigma + x)\frac{\tilde{t}_{\mathbf{k}}^{0S2}}{E_{ct}} + \Sigma_{\mathbf{k}} - \varepsilon_\perp \tag{15}$$

characterizes dispersion for the bonding band, where

$$\Sigma(\mathbf{k}) = \frac{1}{p_\sigma + x}\frac{1}{N} \times \sum_{\mathbf{q}}\left[\left(t_{\mathbf{q}} - p_\sigma J_{\mathbf{k}-\mathbf{q}} - x\frac{\tilde{t}_{\mathbf{q}}^2}{E_{ct}} - (p_\sigma + x)\frac{2\tilde{t}_{\mathbf{q}}\tilde{t}_{\mathbf{k}}}{E_{ct}}\right)K_{\mathbf{q}} + t_\perp(\mathbf{q})K_{\perp\mathbf{q}}\right],$$

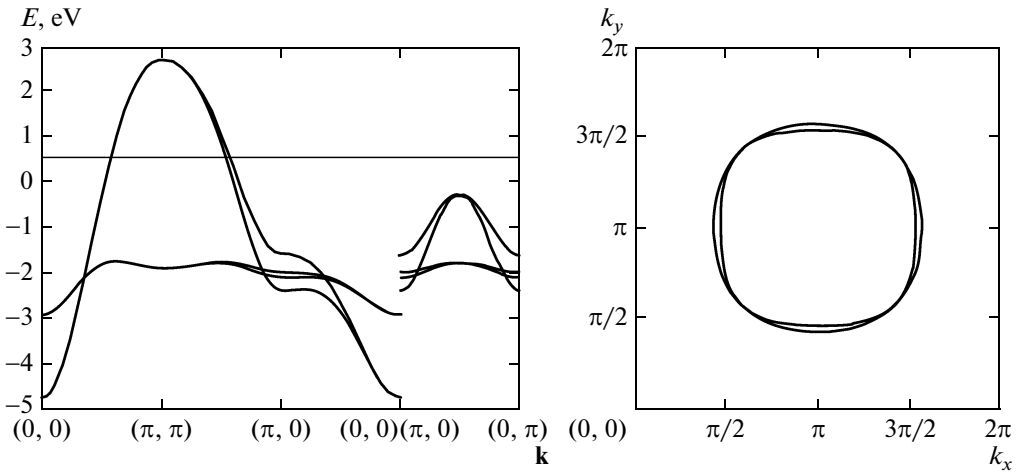

Fig. 9. Band structure (for holes) for the ferromagnetic phase ($T = 10$ K, $H = 300$ T, $x = 0.13$). The broad and narrow bands correspond to up- and down-oriented spins. The horizontal line on the diagram of the band structure shows the chemical potential level.

$K_{\mathbf{q}}$ is the Fourier transform of the kinetic correlators, and $\varepsilon_\perp$ differs from the corresponding expression in zero field in the absence of interlayer spin correlators.

The dispersion of quasiparticle bands with spin σ has the same form except that p_σ changes places with $p_{\bar\sigma}$ and the sign of the Zeeman term changes from minus to plus.

When a high magnetic field is applied, the electronic structure changes from the form shown in Fig. 8 to that in Fig. 9. The band structure is formed by broad bands of mobile quasiparticles with a spin antiparallel to the applied field. The filling factor for such particles has the same values as in the strongly overdoped case of the paramagnetic phase. Thus, the kinetic energy of quasiparticles with such a spin is much higher than the energy of interaction between the spins (antiferromagnetic correlations). Narrow bands resemble in shape the bands of the paramagnetic state, but their width is much smaller.

The reason for the much larger width of the band with the down-oriented spin $\bar\sigma$ as compared to that with spin σ oriented upwards is quite simple. At each lattice site for $x = 0$ in a high magnetic field, all spins are directed upwards. A spin-up hole cannot be added in view of the Pauli principle. And it is only doping that generates Zhang–Rice singlets and makes it possible for spin-up holes to move. Spin fluctuations at a finite temperature play an analogous role. For this reason, the kinetic energy of the holes with spin σ directed upwards is proportional to $x + p_{\bar\sigma} \ll 1$. At the same time, the hole with downward spin $\bar\sigma$ freely moves against the background of the undoped ferromagnetic dielectric state. The situation resembles the spin polaron in a ferromagnetic semiconductor [62, 63]. Since the addition of the second hole to a site forms a Zhang–Rise singlet, this corresponds to the problem of a polaron with the antiferromagnetic exchange interaction between the carrier and the spin. It should also be noted that the band structure in Fig. 9 corresponds to the state of a spin semimetal, in which only states with the same spin projection are present at the Fermi level [64]. In other words, this state is characterized by 100% spin polarization of charge carriers.

The width of the narrow band can be increased either by increasing the number of carriers by doping or as a result of heating. Both these methods lead to an increase in occupation number $p_{\bar\sigma} + x$ for the quasiparticle band with spin σ in proportion to which the kinetic energy of quasiparticles also increases. The chemical potential cannot be intersected by this band for temperatures $T \sim H$. A further increase in the magnetic field induces a number of changes in the topology of the 2D Fermi surface analogous to those upon a change in the doping level. In the case of doping, however, these changes occur due to filling of the band as well as due to a reconstruction of the band structure, while a change in the relation between the temperature and the field modifies only the band topology (to be more precise, the band is broadened as a result of an increase in the fraction of filling of the corresponding state). Prior to significant changes in the topology, only two large hole pockets embedded into each other around (π, π) are present (see Fig. 9). When the values of the field and temperature become close, a number of reconstructions of the Fermi surface can be observed [65, 66]. Indeed, in the case $T \neq 0$ under consideration, we cannot speak of Lifshitz quantum phase transitions because only a smooth crossover is possible. At the first critical point for $H = 150.8$ T ($x = 0.16$, $T = 150$ K), four double embedded hole pockets appear (Fig. 10b). In fact, two transitions take place because double pockets appear as a result of bilayer splitting, but the difference in the critical values of

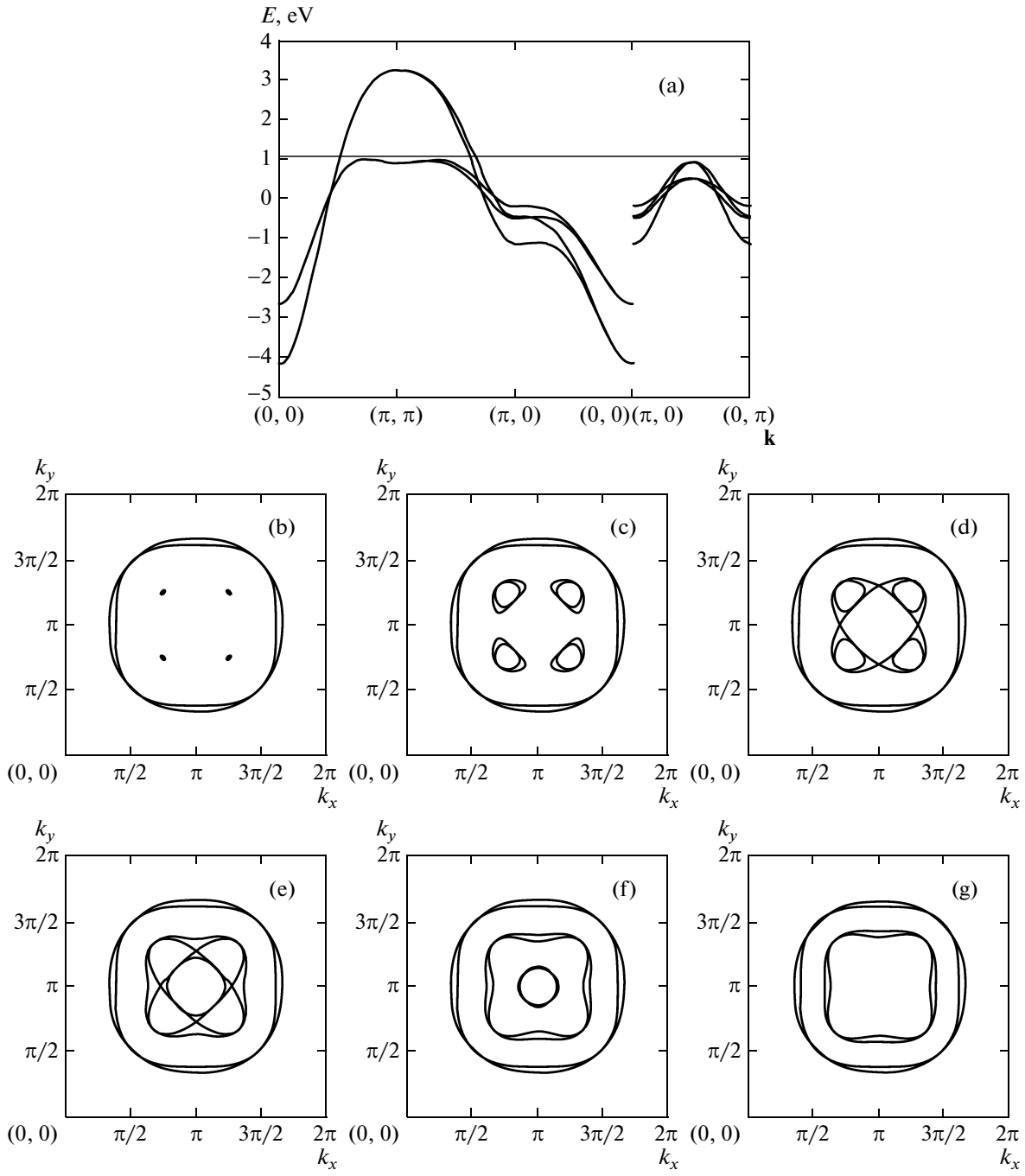

Fig. 10. (a) Band structure ($x = 0.16$, $T = 150$ K, $H = 160$ T); (b–g) evolution of the Fermi surface of $YBa_2Cu_3O_7$ bilayer cuprate upon a change in the H/T ratio: (b) $H = 150.8$ T; (c) $H = 149$ T; (d) $H = 148.3$ T; (e) $H = 147$ T; (f) $H = 145$ T; and (g) $H = 135$ T.

field H for these transitions is so small that it cannot be traced. The central pockets rapidly grow (Fig. 10c) and soon merge into one (Figs. 10d and 10e) at points $H = 148.3$ T and $H = 147$ T with the formation of two inner electron pockets and two outer hole pockets. The electron part of the Fermi surface is rapidly contracted to a point (Fig. 10f) at $H = 140$ T as a result of two (again hardly distinguishable) Lifshitz transitions. As a result, we have two initial hole pockets from the broad band and two hole pockets from the narrow band (Fig. 10g).

6. CONCLUSIONS

Analysis of the normal phase of bilayer cuprates shows that the main effect of tunneling between

CuO_2-planes in a unit cell is the band splitting corresponding to a CuO_2-layer into two bands. This splitting is manifested not only in ARPES experiments as interlayer splitting in the vicinity of antinodal points, but also in the splitting of quantum phase transitions in the hole concentration and in high magnetic field. In our case, the transition in the vicinity of the optimal doping level splits into two transitions with $x_{c1} = 0.14$ and $x_{c2} = 0.18$. The third transition with $x_{c3} = 0.26$ in our calculations is close to the transition at point $x^* = 0.24$ observed in [38]. The two transitions at points x_{c1} and x_{c2} are characterized by a logarithmic singularity in the density of states $N(\varepsilon_F)$ and lead to a singularity of the type $z^2 \ln z$, where $z \sim |x - x_c|$, for the Sommerfeld coefficient in the electron heat capacity $\gamma = C_e/T$ [67], while the transition at points x^* and x_{c3} is accompanied by a jump in $N(\varepsilon_F)$ of the type of a Heaviside step and is a second-order transition in parameter z. Analogously, for transitions in the magnetic field, we can expect a singularity of the $z^2 \ln z$ type, where $z \sim |H - H_c|$, in the electron heat capacity upon a change in the connectivity of the Fermi surface.

ACKNOWLEDGMENTS

This study was supported financially by the program "Quantum Physics of Condensed Media" of the Presidium of the Russian Academy of Sciences (project no. 5.7), the integration projects of the Siberian Branch and the Ural Division of the Russian Academy of Sciences (project no. 40), the Russian Foundation for Basic Research (project no. 09-02-00127), the President of the Russian Federation (grant no. MK-1683.2010.2), and the Federal Target Program P891.

REFERENCES

1. M. Karppinen and H. Yamauchi, Philos. Mag. B **79**, 343 (1999).
2. M. Karppinen and H. Yamauchi, Mater. Sci. Eng., R **26**, 51 (1999).
3. M. Mori, T. Tohyama, and S. Maekawa, J. Phys. Soc. Jpn. **75**, 034708 (2006).
4. A. Trokiner, L. Le Noc, J. Schneck, A. M. Pougnet, R. Mellet, J. Primot, H. Savary, Y. M. Gao, and S. Aubry, Phys. Rev. B: Condens. Matter **44**, 2426 (1991).
5. B. W. Statt and L. M. Song, Phys. Rev. B: Condens. Matter **48**, 3536 (1993).
6. K. Magishi, Y. Kitaoka, G.-Q. Zheng, K. Asayama, K. Tokiwa, A. Iyo, and H. Ihara, J. Phys. Soc. Jpn. **64**, 4561 (1995).
7. G.-q. Zheng, Y. Kitaoka, K. Asayma, K. Hamada, H. Yamauchi, and S. Tanaka, J. Phys. Soc. Jpn. **64**, 3184 (1995).
8. M.-H. Julien, P. Carretta, M. Horvatic, C. Berthier, Y. Berthier, P. Segransan, A. Carrington, and D. Colson, Phys. Rev. Lett. **76**, 4238 (1996).
9. Y. Tokunaga, K. Ishida, and Y. Kitaoka, Phys. Rev. B: Condens. Matter **61**, 9707 (2000).
10. H. Kotegawa, Y. Tokunaga, K. Ishida, G.-Q. Zheng, Y. Kitaoka, H. Kito, A. Iyo, K. Tokiwa, T. Watanabe, and H. Ihara, Phys. Rev. B: Condens. Matter **64**, 064515 (2001).
11. M. Mori and S. Maekawa, Phys. Rev. Lett. **94**, 137003 (2005).
12. S. G. Ovchinnikov and I. S. Sandalov, Physica C (Amsterdam) **161**, 607 (1989).
13. A. F. Barabanov and A. V. Mikheenkov, Fiz. Tverd. Tela (Leningrad) **28** (4), 998 (1986) [Sov. Phys. Solid State **28** (4), 558 (1986)].
14. A. F. Barabanov and A. V. Mikheenkov, Fiz. Tverd. Tela (Leningrad) **30** (4), 1248 (1988) [Sov. Phys. Solid State **30** (4), 728 (1988)].
15. A. F. Barabanov, L. A. Maksimov, and A. V. Mikheenkov, Fiz. Tverd. Tela (Leningrad) **30** (8), 2518 (1988) [Sov. Phys. Solid State **30** (8), 1449 (1988)].
16. V. A. Gavrichkov, S. G. Ovchinnikov, A. A. Borisov, and E. G. Goryachev, Zh. Eksp. Teor. Fiz. **118** (6), 422 (2000) [JETP **91**, (2), 369 (2000)].
17. V. A. Gavrichkov, S. G. Ovchinnikov, and L. E. Yakimov, Zh. Eksp. Teor. Fiz. **129** (6), 1103 (2006) [JETP **102** (6), 972 (2006)].
18. S. G. Ovchinnikov, Yu. S. Orlov, I. Nekrasov, and Z. V. Pchelkina, arXiv:1005.1732v1.
19. B. I. Shraiman and E. D. Siggia, Phys. Rev. Lett. **61**, 467 (1988).
20. S. A. Trugman, Phys. Rev. Lett. **65**, 500 (1990).
21. A. F. Barabanov, R. O. Kuzian, L. A. Maksimov, and G. V. Uimin, Sverkhprovodimost: Fiz., Khim., Tekh. **3**, 8 (1990).
22. A. F. Barabanov, R. O. Kuzian, and L. A. Maksimov, J. Phys.: Condens. Matter. **39**, 129 (1991).
23. A. P. Kampf, Phys. Rep. **249**, 219 (1994).
24. G. Dorf, A. Muramatsu, and W. Hanke, Phys. Rev. B: Condens. Matter **41**, 9264 (1990).
25. A. F. Barabanov, A. A. Kovalev, O. V. Urazaev, A. M. Belemuk, and R. Hayn, Zh. Eksp. Teor. Fiz. **119** (4), 777 (2001) [JETP **92** (4), 677 (2001)].
26. N. M. Plakida and V. S. Oudovenko, Phys. Rev. B: Condens. Matter **59**, 11 949 (1999).
27. V. I. Belinicher, A. L. Chernyshev, and V. A. Shubin, Phys. Rev. B: Condens. Matter **53**, 335 (1996).
28. V. V. Val'kov and D. M. Dzebisashvili, Zh. Eksp. Teor. Fiz. **127** (3), 686 (2005) [JETP **100** (3), 608 (2005)].
29. N. M. Plakida and V. S. Oudovenko, Zh. Eksp. Teor. Fiz. **131** (2), 259 (2007) [JETP **104** (2), 230 (2007)].
30. A. Sherman and M. Schreiber, Phys. Rev. B: Condens. Matter **65**, 134 520 (2002).
31. S. Sachdev, A. V. Chubukov, and A. Sokol, Phys. Rev. B: Condens. Matter **51**, 14 874 (1995).
32. A. V. Chubukov and D. K. Morr, Phys. Rep. **288**, 355 (1997).
33. E. Z. Kuchinskii, I. A. Nekrasov, and M. V. Sadovskii, Pis'ma Zh. Eksp. Teor. Fiz. **82** (4), 217 (2005) [JETP Lett. **82** (4), 198 (2005)].

34. E. Z. Kuchinskii and M. V. Sadovskii, Pis'ma Zh. Eksp. Teor. Fiz. **88** (3), 224 (2008) [JETP Lett. **88** (3), 192 (2008)].

35. M. A. Hossain, J. D. F. Mottershead, D. Fournier, A. Bostwick, J. L. McChesney, E. Rotenberg, R. Liang, W. N. Hardy, G. A. Sawatzky, I. S. Elfimov, D. A. Bonn, and A. Damascelli, Nat. Phys. **4**, 527 (2008).

36. J. Meng, G. Liu, W. Zhang, L. Zhao, H. Liu, X. Jia, D. Mu, S. Liu, X. Dong, J. Zhang, W. Lu, G. Wang, Y. Zhou, Y. Zhu, X. Wang, Z. Xu, C. Chen, and X. J. Zhou, Nature (London) **462**, 335 (2009).

37. R. S. Markiewicz, S. Sahrakorpi, M. Lindroos, H. Lin, and A. Bansil, Phys. Rev. B: Condens. Matter **72**, 054519 (2005).

38. S. G. Ovchinnikov, M. M. Korshunov, and E. I. Shneyder, Zh. Eksp. Teor. Fiz. **136** (5), 898 (2009) [JETP **109** (5), 775 (2009)].

39. I. A. Makarov, S. G. Ovchinnikov, and E. I. Shneyder, Pis'ma Zh. Eksp. Teor. Fiz. **89** (12), 736 (2009) [JETP Lett. **89** (12), 775 (2009)].

40. O. K. Andersen, A. I. Liechtenstein, O. Jepsen, and F. Paulsen, J. Phys. Chem. Solids **56**, 1573 (1995).

41. M. M. Korshunov, V. V. Gavrichkov, S. G. Ovchinnikov, I. A. Nekrasov, Z. V. Pchelkina, and V. I. Anisimov, Phys. Rev. B: Condens. Matter **72**, 165 104 (2005).

42. M. Korshunov and S. Ovchinnikov, Eur. Phys. J. B **57**, 271 (2007).

43. L. N. Bulaevskii, E. L. Nagaev, and D. I. Khomskii, Zh. Eksp. Teor. Fiz. **54** (5), 1562 (1968) [Sov. Phys. JETP **27** (5), 836 (1968)].

44. K. A. Chao, J. Spalek, and A. M. Oles, J. Phys. C: Solid State Phys. **10**, L271 (1977).

45. J. E. Hirsch, Phys. Rev. Lett. **54**, 1317 (1985).

46. V. I. Belinicher, A. L. Chernyshev, and V. A. Shubin, Phys. Rev. B: Condens. Matter **53**, 335 (1996).

47. N. M. Plakida and V. S. Oudovenko, Phys. Rev. B: Condens. Matter **59**, 11 949 (1999).

48. R. Hayn, A. F. Barabanov, and J. Schulenburg, Z. Phys. B: Condens. Matter **102**, 359 (1997).

49. V. V. Val'kov and D. M. Dzebisashvili, Zh. Eksp. Teor. Fiz. **127** (3), 686 (2005) [JETP **100** (3), 608 (2005)].

50. R. O. Kuzian, R. Hayn, A. F. Barabanov, and L. A. Maksimov, Phys. Rev. B: Condens. Matter **58**, 6194 (1998).

51. D. L. Feng, N. P. Armitage, D. H. Lu, A. Damascelli, J. P. Hu, P. Bogdanov, A. Lanzara, F. Ronning, K. M. Shen, H. Eisaki, C. Kim, Z.-X. Shen, J.-I. Shimoyama, and K. Kishio, Phys. Rev. Lett. **86**, 5550 (2001).

52. Y.-D. Chuang, A. D. Gromko, and A. Fedorov, Phys. Rev. Lett. **87**, 117 002 (2001).

53. A. A. Kordyuk, S. V. Borisenko, M. S. Golden, S. Legner, K. A. Nenkov, M. Knupfer, J. Fink, H. Berger, L. Forro, and R. Follath, Phys. Rev. B: Condens. Matter **66**, 014 502 (2002).

54. S. Sahrakorpi, M. Lindroos, R. S. Markiewicz, and A. Bansil, Phys. Rev. Lett. **95**, 157 601 (2005).

55. T. Kondo, R. Khasanov, Y. Sassa, A. Bendounan, J. Chang, J. Mesot, H. Keller, N. D. Zhigadlo, M. Shi, Z. Bukowski, J. Karpinski, and A. Kaminski, Phys. Rev. B: Condens. Matter **80**, 100 505 (2009).

56. A. Kaminski, S. Rosenkranz, H. M. Fretwell, M. R. Norman, M. Randeria, J. C. Campuzano, J.-M. Park, Z. Z. Li, and H. Raffy, Phys. Rev. B: Condens. Matter **73**, 174 511 (2006).

57. J. M. Tranquada, D. E. Cox, W. Kunnmann, H. Moudden, G. Shirane, M. Suenaga, P. Zolliker, D. Vaknin, S. K. Sinha, M. S. Alvarez, A. J. Jacobson, and D. C. Johnston, Phys. Rev. Lett. **60**, 156 (1988).

58. N. Doiron-Leyraud, C. Proust, D. LeBoeuf, J. Levallois, J.-B. Bonnemaison, R. Liang, D. A. Bonn, W. N. Hardy, and L. Taillefer, Nature (London) **447**, 565 (2007).

59. A. Audouard, C. Jaudet, D. Vignolles, R. Liang, D. A. Bonn, W. N. Hardy, L. Taillefer, and C. Proust, Phys. Rev. Lett. **103**, 157 003 (2009).

60. A. F. Barabanov, L. A. Maksimov, and L. E. Zhukov, Physica C (Amsterdam) **212**, 375 (1993).

61. D. LeBoeuf, N. Doiron-Leyraud, J. Levallois, R. Daou, J.-B. Bonnemaison, N. E. Hussey, L. Balicas, B. J. Ramshaw, R. Liang, D. A. Bonn, W. N. Hardy, S. Adachi, C. Proust, and L. Taillefer, Nature (London) **450**, 533 (2007).

62. E. L. Nagaev, Zh. Eksp. Teor. Fiz. **56** (3), 1013 (1969) [Sov. Phys. JETP **29** (3), 545 (1969)].

63. Yu. A. Izyumov and M. V. Medvedev, Zh. Eksp. Teor. Fiz. **59**, 553 (1970) [Sov. Phys. JETP **32**, 302 (1970)].

64. V. Yu. Irkhin and M. I. Katsnel'son, Usp. Fiz. Nauk **164** (7), 705 (1994) [Phys.—Usp. **37** (7), 659 (1994)].

65. I. M. Lifshitz, Zh. Eksp. Teor. Fiz. **38**, 1569 (1960) [Sov. Phys. JETP **11**, 1130 (1960)].

66. I. M. Lifshitz, M. Ya. Azbel', and M. I. Kaganov, *Electron Theory of Metals* (Nauka, Moscow, 1971; Consultants Bureau, New York, 1973).

67. S. G. Ovchinnikov, E. I. Shneyder, and M. M. Korshunov, arXiv:0908.0576.

Translated by N. Wadhwa